Pseudomagnetic fields in square lattices

Junsong Sun,[1] Xingchuan Zhu,[2] Tianyu Liu,[3,4,*] Shiping Feng,[5] and Huaiming Guo[1,†]

[1]*School of Physics, Beihang University, Beijing 100191, China*

[2]*Interdisciplinary Center for Fundamental and Frontier Sciences, Nanjing University of Science and Technology, Jiangyin, Jiangsu 214443, People's Republic of China*

[3]*Shenzhen Institute for Quantum Science and Engineering and Department of Physics, Southern University of Science and Technology (SUSTech), Shenzhen 518055, China*

[4]*International Quantum Academy, Shenzhen 518048, China*

[5]*Department of Physics, Beijing Normal University, Beijing 100875, China*

(Received 29 August 2023; revised 7 November 2023; accepted 9 November 2023; published 27 November 2023)

We have investigated the effects of strain on two-dimensional square lattices and examined the methods for inducing pseudomagnetic fields. In both the columnar and staggered π-flux square lattices, we have found that strain only modulates Fermi velocities rather than inducing pseudomagnetic fields. However, spatially nonuniform on-site potentials (anisotropic hoppings) can create pseudomagnetic fields in columnar (staggered) π-flux square lattices. On the other hand, we demonstrate that strain does induce pseudomagnetic fields in staggered zero-flux square lattices. By breaking a quarter of the bonds, we clarify that a staggered zero-flux square lattice is topologically equivalent to a honeycomb lattice and displays pseudovector potentials and pseudo-Landau-levels at the Dirac points.

DOI: 10.1103/PhysRevB.108.205149

I. INTRODUCTION

Strain engineering has emerged as a powerful tool in condensed matter physics for manipulating the electronic properties of Dirac materials. In graphene, specifically, the application of strain [1] can generate a pseudomagnetic field [2–9] that couples to the two-dimensional Dirac electrons in a manner similar to an externally applied magnetic field. Numerous experimental [10–16] and theoretical [17–21] studies have identified in graphene such strain-induced pseudomagnetic fields, which give rise to novel transport phenomena such as chiral anomalies [9,20] and quantum oscillations [21] in the absence of magnetic fields.

Beyond graphene, pseudomagnetic fields can also be induced in various other materials, including superconducting [22–25], magnonic [26–31], photonic [32], and acoustic [33–35] materials, as long as they possess a Dirac cone band structure. In the case of two-dimensional materials, strain-induced pseudomagnetic fields have previously been predicted only in honeycomb-like lattices (e.g., honeycomb [36–39], kagome [40], and α-T_3 [41,42] lattices), because their lattice geometry inherently guarantees the presence of Dirac cones. However, it remains unknown whether strain can induce pseudomagnetic fields in non-honeycomb-like lattices.

Square lattices are well-known for exhibiting Dirac cones in the low-energy band structure when each elementary plaquette hosts half a magnetic flux quantum. Due to this unique band structure, the π-flux square lattices have attracted significant attention and have been extensively studied in both noninteracting [43–45] and strongly correlated [46–50] regimes. Furthermore, the presence of Dirac cones in π-flux square lattices is a prerequisite for the emergence of strain-induced pseudomagnetic fields. Therefore, it is intriguing and worthwhile to investigate whether a strained π-flux square lattice can indeed give rise to a pseudomagnetic field, which may have potential experimental realizations in optical lattices [51,52] or electrical circuits [53].

In this manuscript, we investigate the effects of strain on two-dimensional square lattices with and without π-flux. We examine two different configurations of π-flux, and we observe that strain alone does not result in the induction of a pseudomagnetic field in either case. However, we discover that spatially nonuniform on-site potentials or anisotropic hoppings can serve as alternative sources for generating pseudomagnetic fields. For the case without π-flux, we observe that Dirac cones can be produced by introducing staggered hoppings along the y direction. Additionally, we find that strain patterns commonly used in graphene have the ability to induce pseudomagnetic fields in this system. In the limit case in which the weak bonds in the y direction are eliminated, the resulting brick-wall square lattice is topologically equivalent to a honeycomb lattice. Interestingly, the pseudomagnetic field induced by strain persists in this transformed square geometry. These findings expand the effect of strain to square geometries, further deepening our comprehension of the strain-induced pseudomagnetic field.

This paper is organized as follows. In Sec. II, we introduce the columnar π-flux square lattice and demonstrate its low-energy Dirac cone band structure. In Sec. III, we show that strain only modulates the Fermi velocity of the columnar

*liuty@sustech.edu.cn
†hmguo@buaa.edu.cn

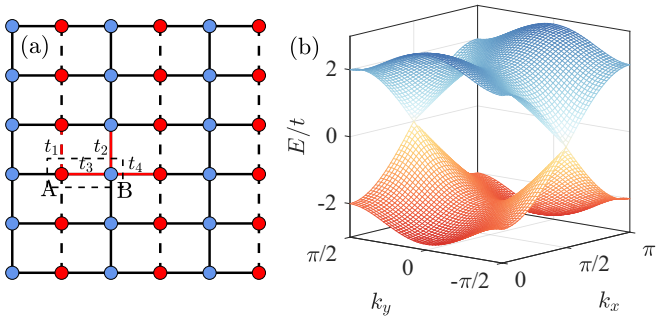

FIG. 1. (a) Schematic plot of a columnar π-flux square lattice. Each unit cell consists of two sites, labeled as A (red) and B (blue), respectively. The hopping parameters of the four bonds associated with each unit cell are labeled as $t_{1,2,3,4}$. (b) Band structure of the nearest-neighbor tight-binding model [Eq. (1)] defined on the columnar π-flux square lattice. Here we have adopted $-t_1 = t_2 = t_3 = t_4 = t$.

π-flux square lattice without inducing a pseudomagnetic field. In Sec. IV, we propose that a pseudomagnetic field can arise when a spatially nonuniform on-site potential is introduced to the columnar π-flux square lattice. In Sec. V, we find that strain cannot induce a pseudomagnetic field in the staggered π-flux square lattice, but spatially nonuniform anisotropic hoppings may generate one. In Sec. VI, we demonstrate that strain can induce a pseudomagnetic field in the staggered zero-flux square lattice. In Sec. VII, we reveal that breaking a quarter of bonds in the staggered zero-flux square lattice results in topological equivalence to a honeycomb lattice, exhibiting a strain-induced pseudomagnetic field. Finally, in Sec. VIII, we provide a summary of our key findings and conclude the paper.

II. COLUMNAR π-FLUX SQUARE LATTICE

With half of a magnetic flux quantum threading through each plaquette of a square lattice, the hopping parameters associated with the four edges of the plaquette acquire Aharonov-Bohm phases that sum up to π. By assigning this π phase to t_1, the square lattice manifests a columnar pattern with a bipartite unit cell [Fig. 1(a)]. The corresponding spinless nearest-neighbor tight-binding Hamiltonian is given by

$$H_0 = \sum_{\boldsymbol{r}} (t_1 a_{\boldsymbol{r}}^\dagger a_{\boldsymbol{r}+\boldsymbol{\delta}_2} + t_2 b_{\boldsymbol{r}}^\dagger b_{\boldsymbol{r}+\boldsymbol{\delta}_2} + t_3 a_{\boldsymbol{r}}^\dagger b_{\boldsymbol{r}} + t_4 a_{\boldsymbol{r}}^\dagger b_{\boldsymbol{r}-2\boldsymbol{\delta}_1}) + \text{H.c.}, \tag{1}$$

where $a_{\boldsymbol{r}}$ and $b_{\boldsymbol{r}}$ are the annihilation operators associated with the two sublattices, and $\boldsymbol{\delta}_1 = (1, 0)$ and $\boldsymbol{\delta}_2 = (0, 1)$ are the nearest-neighbor vectors with the lattice constant set to unity. The hopping parameters [Fig. 1(a)] associated with each unit cell satisfy $-\text{sgn}(t_1) = \text{sgn}(t_2) = \text{sgn}(t_3) = \text{sgn}(t_4)$. In momentum space and the sublattice basis $\psi_{\boldsymbol{k}} = (a_{\boldsymbol{k}}, b_{\boldsymbol{k}})^T$, the Hamiltonian [Eq. (1)] can be written as $H_0 = \sum_{\boldsymbol{k}} \psi_{\boldsymbol{k}}^\dagger \mathcal{H}_{\boldsymbol{k}} \psi_{\boldsymbol{k}}$ with the kernel given by

$$\mathcal{H}_{\boldsymbol{k}} = \begin{bmatrix} 2t_1 \cos(k_y) & t_3 + t_4 e^{2ik_x} \\ t_3 + t_4 e^{-2ik_x} & 2t_2 \cos(k_y) \end{bmatrix}. \tag{2}$$

Taking $-t_1 = t_2 = t_3 = t_4 = t$, the band structure of $\mathcal{H}_{\boldsymbol{k}}$ reads $E_{\boldsymbol{k}} = \pm 2t\sqrt{\cos^2(k_x) + \cos^2(k_y)}$, which exhibits two Dirac points at $\boldsymbol{K}^\xi = (\frac{\pi}{2}, \xi\frac{\pi}{2})$ with $\xi = \pm$ [see Fig. 1(b)]. We expand $\mathcal{H}_{\boldsymbol{k}}$ in the vicinity of $\boldsymbol{K}^\xi$ and obtain the corresponding low-energy effective Hamiltonian

$$H_{\boldsymbol{q}}^\xi = 2t \begin{bmatrix} \xi q_y & -iq_x \\ iq_x & -\xi q_y \end{bmatrix} = 2t(\xi \sigma_z q_y + \sigma_y q_x), \tag{3}$$

where σ_y and σ_z are Pauli matrices. As a consequence, a linear dispersion relation with isotropic properties emerges in the vicinity of the Dirac points, expressed as $\varepsilon_{\boldsymbol{q}} = \pm 2t\sqrt{q_x^2 + q_y^2}$.

III. STRAIN-MODULATED FERMI VELOCITY IN THE COLUMNAR π-FLUX SQUARE LATTICE

We now study the strain effects in the columnar π-flux square lattice. When the strain is applied, it deforms the lattice and modulates the hopping parameters to

$$t_n = t + \delta t_n, \tag{4}$$

where δt_n denotes the correction to the nth hopping parameter. Any strain, regardless of its space dependence, can be characterized by a displacement field $\boldsymbol{U}(\boldsymbol{R})$. The variation δt_n can be approximated in terms of the strain tensor $u_{ij} = (\partial_i U_j + \partial_j U_i)/2$ and the corresponding bond vector $\boldsymbol{\delta}_n$ as

$$\delta t_n = -\beta t \boldsymbol{\delta}_n \cdot \boldsymbol{u} \cdot \boldsymbol{\delta}_n, \tag{5}$$

where β is referred to as the Grüneisen parameter [3]. For the columnar π-flux square lattice, the strain-modulated hopping parameters thus read

$$\begin{aligned} t_{1,2} &= \pm t(1 - \beta \boldsymbol{\delta}_2 \cdot \boldsymbol{u} \cdot \boldsymbol{\delta}_2), \\ t_{3,4} &= t(1 - \beta \boldsymbol{\delta}_1 \cdot \boldsymbol{u} \cdot \boldsymbol{\delta}_1), \end{aligned} \tag{6}$$

where the plus (minus) sign in the first equation corresponds to t_2 (t_1). According to Eq. (6), we always have $t_1 = -t_2$ and $t_3 = t_4$ regardless of the form of $\boldsymbol{U}(\boldsymbol{R})$. Plugging Eq. (6) into Eq. (2) and expanding around $\boldsymbol{K}^\xi$, we find that the low-energy effective Hamiltonian [Eq. (3)] is adapted to

$$H_{\boldsymbol{q}}^\xi = 2t[\xi \sigma_z (1 - \beta \boldsymbol{\delta}_2 \cdot \boldsymbol{u} \cdot \boldsymbol{\delta}_2) q_y + \sigma_y (1 - \beta \boldsymbol{\delta}_1 \cdot \boldsymbol{u} \cdot \boldsymbol{\delta}_1) q_x], \tag{7}$$

which only incorporates modulation of the Fermi velocity instead of induction of a pseudomagnetic field. For spatially uniform strain, the Fermi velocity remains constant and exhibits anisotropy when $\boldsymbol{\delta}_1 \cdot \boldsymbol{u} \cdot \boldsymbol{\delta}_1 \neq \boldsymbol{\delta}_2 \cdot \boldsymbol{u} \cdot \boldsymbol{\delta}_2$. For nonuniform strain, the Fermi velocity in general exhibits anisotropy and spatial inhomogeneity simultaneously.

It is well known that strain in graphene can induce both an inhomogeneous Fermi velocity and a pseudomagnetic field, which together give rise to dispersive pseudo-Landau-levels [9,21]. However, in the case of the columnar π-flux square lattice, nonuniform strain only generates an inhomogeneous Fermi velocity. It is thus anticipated that an external magnetic field produces dispersive Landau levels. In this scenario, the magnetic field $\boldsymbol{B} = B\hat{z}$ is responsible for the Landau quantization $E_n = \sqrt{2neB\hbar v_x v_y}$ as illustrated in Fig. 2(a), while the nonuniform Fermi velocity $\boldsymbol{v} = (v_x, v_y)$ becomes $\boldsymbol{k}$-dependent when Fourier-transformed into momentum space, resulting in

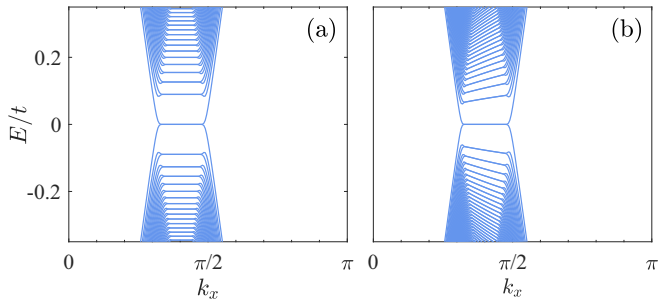

FIG. 2. Band structure of the nearest-neighbor tight-binding model on the columnar π-flux square lattice with an ordinary magnetic field. (a) Flat Landau levels. (b) Dispersive Landau levels in the presence of a nonuniform uniaxial strain. The strain results from the displacement field $\boldsymbol{U} = (0, \frac{c}{2\beta}y^2)$ with strength $c/c_{\max} = 0.5$ ($c_{\max} = 1/L_y$). The lattice used in the calculation has a finite width ($L_y = 600$) in the y direction and is infinite along the x direction.

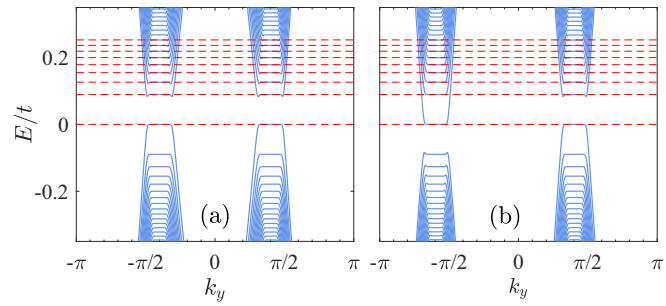

FIG. 3. The low-energy band structure of the nearest-neighbor tight-binding model of the columnar π-flux square lattice. (a) Pseudo-Landau-levels induced by the engineered nonuniform on-site potential [Eq. (8)]. (b) Landau levels arising from a real magnetic field $B = U_0$. The red curves in (a) and (b) represent the analytical Landau levels [Eq. (10)].

dispersion. Our claim is numerically substantiated with a displacement field $\boldsymbol{U} = (0, \frac{c}{2\beta}y^2)$ through exact diagonalization. Indeed, we find that the initially flat Landau levels [Fig. 2(a)] become dispersive [Fig. 2(b)] due to the nonuniform Fermi velocity modulated by the strain.

Previously, there has been a debate regarding the origin of the dispersive pseudo-Landau-levels in graphene. Recent findings [21] have revealed that the dispersion arises from both the strain-modulated inhomogeneous Fermi velocity [9,54] and the strain-induced nonuniform pseudomagnetic field [20]. In fact, these two effects cannot be separated for strong strain [21]. In contrast, in the columnar π-flux square lattice, strain independently affects the Fermi velocity and thus can serve as a more agile tuning knob of the electronic structure.

IV. ON-SITE POTENTIAL INDUCED PSEUDOMAGNETIC FIELD IN THE COLUMNAR π-FLUX SQUARE LATTICE

In Sec. III, we have shown that the strain-modulated hopping parameters are unable to generate a pseudomagnetic field on the columnar π-flux square lattice. Nevertheless, upon analyzing the structure of the low-energy effective Hamiltonian [Eq. (3)], it is observed that a nonuniform on-site potential, which varies with the x coordinate, has the ability to induce a vector potential. Explicitly, the potential reads

$$H_1 = 2tU_0 \sum_{\boldsymbol{r}} (\boldsymbol{r}\cdot\hat{x})(a_{\boldsymbol{r}}^\dagger a_{\boldsymbol{r}} - b_{\boldsymbol{r}}^\dagger b_{\boldsymbol{r}}), \tag{8}$$

where U_0 characterizes the strength of the potential. The total Hamiltonian now becomes $H_{\rm tot} = H_0 + H_1$, whose low-energy effective Hamiltonian [cf., Eq. (3)] is written as

$$\begin{aligned} H_{\boldsymbol{q}}^{\xi} &= 2t\begin{bmatrix} \xi q_y + U_0 x & -iq_x \\ iq_x & -\xi q_y - U_0 x \end{bmatrix} \\ &= 2t[\xi\sigma_z(q_y + \xi U_0 x) + \sigma_y q_x]. \end{aligned} \tag{9}$$

It is worth noting that H_1 is an artificial term, similar to an electric field, but experienced oppositely by the two sublattices. The Hamiltonian [Eq. (9)] exhibits a vector potential $\boldsymbol{A}^{\xi} = (0, \xi U_0 x)$, which has opposite signs at the two Dirac points. Solving the eigenvalue problem of Eq. (9) yields the pseudo-Landau-levels (see Appendix A for details)

$$E_n = \pm 2t\sqrt{2U_0 n}, \quad n = 0, 1, 2, \ldots, \tag{10}$$

which exhibit a $\sqrt{n}$ dependence, similar to that in strained graphene. The analytical dispersion [Eq. (10)] can be further verified by diagonalizing the corresponding tight-binding model on the columnar π-flux square lattice, with open (periodic) boundary condition along the x (y) direction. As shown in Fig. 3(a), the analytical pseudo-Landau-levels and the numerical bands match quite well with each other near the Dirac points. For comparison, we also plot in Fig. 3(b) the Landau levels induced by a real magnetic field with the same strength (i.e., $B = U_0$). While the pseudo-Landau-levels at the two Dirac points are linked by the time-reversal symmetry, the two sets of Landau levels in Fig. 3(b) are related to each other by the inversion symmetry.

V. STAGGERED π-FLUX SQUARE LATTICE

We have so far focused on the columnar π-flux square lattice in Secs. II–IV. In the present section, we analyze a different π-flux square lattice which illustrates a staggered pattern [Fig. 4(a)]. We will examine the strain effects and study the possible induction of pseudomagnetic fields.

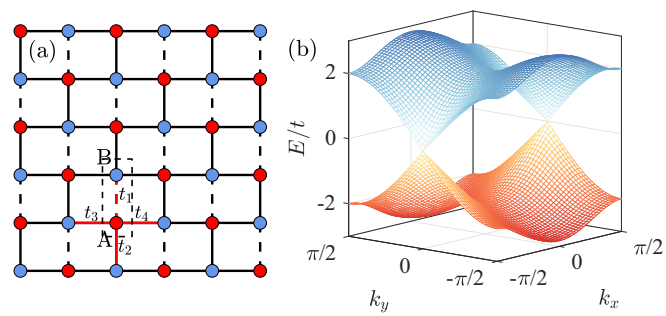

FIG. 4. (a) Schematic plot of a staggered π-flux square lattice. Each unit cell consists of two sites, labeled as A (red) and B (blue), respectively. The hopping parameters of the four bonds associated with each unit cell are labeled as $t_{1,2,3,4}$. (b) Band structure of the tight-binding model [Eq. (11)] defined on the staggered π-flux square lattice. Here we have adopted $-t_1 = t_2 = t_3 = t_4 = t$.

The tight-binding model of a staggered π-flux square lattice reads

$$H_0 = \sum_{\boldsymbol{r}} (t_1 a_{\boldsymbol{r}}^\dagger b_{\boldsymbol{r}} + t_2 a_{\boldsymbol{r}}^\dagger b_{\boldsymbol{r}-2\boldsymbol{\delta}_2} + t_3 a_{\boldsymbol{r}}^\dagger b_{\boldsymbol{r}-\boldsymbol{\delta}_1-\boldsymbol{\delta}_2} + t_4 a_{\boldsymbol{r}}^\dagger b_{\boldsymbol{r}+\boldsymbol{\delta}_1-\boldsymbol{\delta}_2}) + \text{H.c.} \tag{11}$$

Performing Fourier transform, we find in the sublattice space the following Bloch Hamiltonian:

$$\mathcal{H}_{\boldsymbol{k}} = \begin{bmatrix} 0 & f_{\boldsymbol{k}} \\ f_{\boldsymbol{k}}^* & 0 \end{bmatrix}, \tag{12}$$

where $f_{\boldsymbol{k}} = t_1 + t_2 e^{-\mathrm{i}2k_y} + t_3 e^{-\mathrm{i}(k_x+k_y)} + t_4 e^{\mathrm{i}(k_x-k_y)}$. Taking $-t_1 = t_2 = t_3 = t_4 = t$, we find that $\mathcal{H}_{\boldsymbol{k}}$ exhibits two Dirac points at $\boldsymbol{K}^\xi = (\xi\frac{\pi}{2}, 0)$ [see Fig. 4(b)], in the vicinity of which the low-energy effective Hamiltonian is obtained through linearization as

$$H_{\boldsymbol{q}}^\xi = -2t(\sigma_x \xi q_x - \sigma_y q_y), \tag{13}$$

whose spectrum $\varepsilon_{\boldsymbol{q}} = \pm 2t\sqrt{q_x^2 + q_y^2}$ is exactly the same as that of the columnar π-flux square lattice.

We next consider the effect of strain in the staggered π-flux square lattice. The strain can be incorporated using the same hopping modulation [Eq. (6)]. Plugging Eq. (6) into Eq. (11), performing Fourier transform, and linearizing in the vicinity of the Dirac points, we find the low-energy effective Hamiltonian

$$H_{\boldsymbol{q}}^\xi = -2t\xi\sigma_x(1 - \beta\boldsymbol{\delta}_1 \cdot \boldsymbol{u} \cdot \boldsymbol{\delta}_1)q_x + 2t\sigma_y(1 - \beta\boldsymbol{\delta}_2 \cdot \boldsymbol{u} \cdot \boldsymbol{\delta}_2)q_y. \tag{14}$$

It is apparent that applying nonuniform strain only results in an inhomogeneous Fermi velocity and cannot produce a pseudomagnetic field. This observation is consistent with the strain effect in the columnar π-flux square lattice.

While a pseudomagnetic field cannot be produced by strain, it can be artificially created through engineering the hopping parameters. One such example reads

$$t_1 = -t,\ t_2 = t_4 = t,\ t_3 = t(1 - cx), \tag{15}$$

where c characterizes the inhomogeneous anisotropy of hoppings. The resulting low-energy effective Hamiltonian becomes

$$H_{\boldsymbol{q}}^\xi = 2t\left[-\left(1 - \frac{c}{2}x\right)\xi q_x\sigma_x + \left(q_y - \xi\frac{c}{2}x\right)\sigma_y\right]. \tag{16}$$

Clearly, a pseudovector potential $\boldsymbol{A}^\xi = (0, \xi\frac{c}{2}x)$ with opposite signs $\xi = \pm$ is created at the two Dirac points, resulting in a uniform pseudomagnetic field in the z direction. Solving the eigenvalue problem of Eq. (16) yields the pseudo-Landau-levels (see Appendix B for details)

$$E_n^\xi = \pm 2t\sqrt{n|c|(1 - \xi q_y)}, \quad n = 0, 1, 2, \ldots, \tag{17}$$

where the dispersion of the pseudo-Landau-levels is originated from the combined effect of the nonuniform pseudomagnetic field and Fermi velocity. The analytically derived pseudo-Landau-levels [Eq. (17)] well match the numerical energy bands obtained through exact diagonalization of the nearest-neighbor tight-binding model on the staggered π-flux square lattice [Fig. 5(a)]. The dispersion of the pseudo-Landau-levels makes them stand out from the regular flat Landau levels [Fig. 5(b)] produced by a real magnetic field.

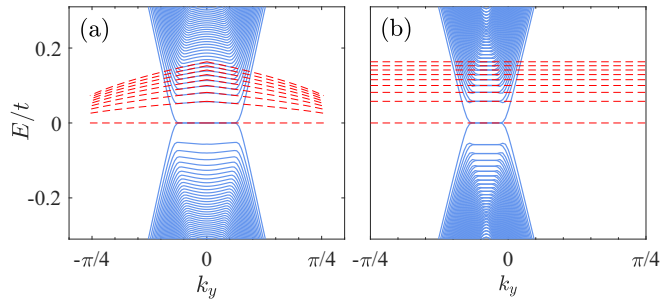

FIG. 5. The low-energy band structure of the nearest-neighbor tight-binding model on the staggered π-flux square lattice. (a) Pseudo-Landau-levels induced by the engineered hopping parameters [Eq. (15)]. The anisotropic hoppings are characterized by $c = 0.5c_{\max}$, where $c_{\max} = 1/L_x$. (b) Landau levels arising from a real magnetic field $B = c/2$. In both panels, the red curves represent the analytical Landau levels [Eq. (17)], and the system size is $L_x = 600$ (infinite) in the x (y) direction.

We mention that the zeroth pseudo-Landau-levels [Eq. (17)] generated by engineering the hopping parameters [Eq. (15)] also exhibit sublattice polarization, and they are different from the ordinary zeroth Landau levels that distribute on both sublattices. To substantiate this claim, we plot the distributions of the wave functions at the two valleys (i.e., Dirac cones). The zeroth pseudo-Landau-levels are only distributed on the B sublattice for $c > 0$ at both valleys [Figs. 6(a) and 6(b)]. In contrast, the zeroth Landau levels can appear on either the A or B sublattice [Figs. 6(c) and 6(d)], depending on which valley is examined. It is worth noting that the sublattice polarization flips when the sign of c is reversed.

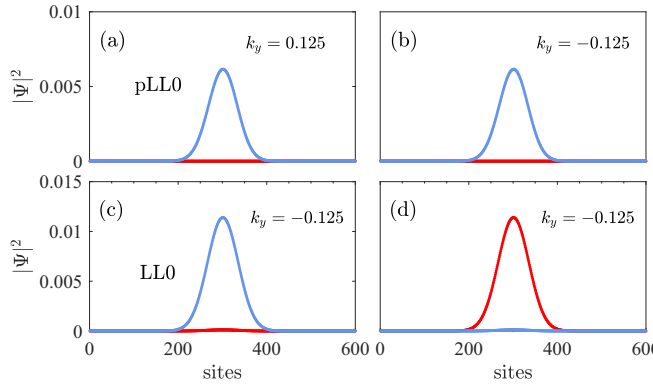

FIG. 6. The distributions of the wave functions of zeroth (pseudo-)Landau-levels at different momenta. (a) Zeroth pseudo-Landau-level at $k_y = 0.125$. (b) Zeroth pseudo-Landau-level at $k_y = -0.125$. (c),(d) Two degenerate sectors of the zeroth Landau levels at $k_y = -0.125$. The degeneracy emerges because the two Dirac cones, whose Dirac points are located at $\boldsymbol{K}^\xi = (\xi\frac{\pi}{2}, 0)$, overlap in the vicinity of $k_y = 0$ when projected along the x direction. For all panels, the red (blue) curves represent the distribution on the A (B) sublattice. Here we set $c = 0.5c_{\max}$.

VI. STRAIN-INDUCED PSEUDOMAGNETIC FIELD IN THE STAGGERED ZERO-FLUX SQUARE LATTICE

In Sec. V, we have shown that strain only modulates the Fermi velocity of the staggered π-flux square lattice. In the present section, we demonstrate that strain may induce a pseudomagnetic field if the flux is removed [i.e., $\mathrm{sgn}(t_1) = \mathrm{sgn}(t_2) = \mathrm{sgn}(t_3) = \mathrm{sgn}(t_4)$] from the staggered π-flux square lattice. The circumvention of the negative hopping should also render the lattice more experimentally accessible.

Removing the flux, the resulting staggered zero-flux square lattice can still be characterized by the tight-binding Hamiltonian [Eq. (11)] and the Bloch Hamiltonian [Eq. (12)] of the staggered π-flux square lattice [Fig. 4(a)], except that we now take $t_1 = rt$ and $t_2 = t_3 = t_4 = t$ rather than $-t_1 = t_2 = t_3 = t_4 = t$. For the ratio $0 \leqslant r < 1$, we find for the Bloch Hamiltonian [Eq. (12)] two gapless points at $\boldsymbol{K}^\xi = [\xi \arccos(-\frac{1+r}{2}), 0]$. Expanding the Bloch Hamiltonian [Eq. (12)] in the vicinity of $\boldsymbol{K}^\xi$ yields a low-energy effective Hamiltonian

$$H_{\boldsymbol{q}}^\xi = -\sigma_x t \xi p q_x + \sigma_y t[(1-r)q_y - \xi p q_x q_y], \tag{18}$$

where we define $p = \sqrt{(3+r)(1-r)}$ for transparency. We note that Eq. (18) is still a Dirac Hamiltonian when ignoring the $O(q_x q_y)$ term.

We now check whether such Dirac cones can be Landau-quantized by strain. By incorporating the corrections to the hopping parameters [Eq. (6)], we can derive the low-energy effective Hamiltonian in the presence of strain as

$$\begin{aligned} H_{\boldsymbol{q}}^\xi = {} & \sigma_x t\{-\xi p(1-\beta\boldsymbol{\delta}_1\cdot\boldsymbol{u}\cdot\boldsymbol{\delta}_1)q_x \\ & + (1+r)\beta(\boldsymbol{\delta}_1\cdot\boldsymbol{u}\cdot\boldsymbol{\delta}_1 - \boldsymbol{\delta}_2\cdot\boldsymbol{u}\cdot\boldsymbol{\delta}_2)\} \\ & + \sigma_y t\{[(1-r) + (1+r)\beta\boldsymbol{\delta}_1\cdot\boldsymbol{u}\cdot\boldsymbol{\delta}_1 \\ & - 2\beta\boldsymbol{\delta}_2\cdot\boldsymbol{u}\cdot\boldsymbol{\delta}_2]q_y - \xi p(1-\beta\boldsymbol{\delta}_1\cdot\boldsymbol{u}\cdot\boldsymbol{\delta}_1)q_x q_y\}, \end{aligned} \tag{19}$$

which indicates that a uniform pseudomagnetic field can be induced when $\boldsymbol{\delta}_1\cdot\boldsymbol{u}\cdot\boldsymbol{\delta}_1 - \boldsymbol{\delta}_2\cdot\boldsymbol{u}\cdot\boldsymbol{\delta}_2$ is proportional to the y coordinate. This requirement can be fulfilled by a nonuniform uniaxial strain characterized by the displacement field $\boldsymbol{U} = (0, \frac{c}{2\beta}y^2)$. Under this strain, the low-energy effective Hamiltonian can be expressed as

$$\begin{aligned} H_{\boldsymbol{q}}^\xi = {} & t\{\sigma_x[-\xi p q_x - (1+r)cy] \\ & + \sigma_y[(1-r-2cy)q_y - \xi p q_x q_y]\}. \end{aligned} \tag{20}$$

Solving the eigenvalue problem of Eq. (20) yields the following strain-induced dispersive pseudo-Landau-levels (see Appendix C for details):

$$E_n^\xi = \pm t\sqrt{2(1-r)}\sqrt{n|c|(\xi p q_x + 1 + r)}, \tag{21}$$

which exhibit a good match to the numerical band structure obtained by diagonalizing the nearest-neighbor tight-binding model that incorporates the strain effect [Figs. 7(a) and 7(b)]. From Eq. (21), it can be inferred that the interval between the pseudo-Landau-levels decreases as r increases from 0 to 1. Specifically, when $r = 1$, the pseudo-Landau-levels collapse, because the ordinary square lattice is restored and the low-energy dispersion becomes quadratic.

A pseudomagnetic field can also be generated by applying a triaxial strain, which is characterized by the displacement field $\boldsymbol{U}(x,y) = \frac{c}{\beta}(2xy, x^2 - y^2)$. According to Eq. (6), the hopping parameters are modulated by the triaxial strain as

$$t_1 = rt(1+2cy),\ t_2 = t(1+2cy),\ t_3 = t_4 = t(1-2cy). \tag{22}$$

The low-energy effective Hamiltonian can be directly obtained and reads

$$\begin{aligned} H_{\boldsymbol{q}}^\xi = {} & t\sigma_x[-\xi p(1-2cy)q_x + (1+r)4cy] \\ & + t\sigma_y[1-r-\xi p q_x + 2c(3+r)y]q_y. \end{aligned} \tag{23}$$

We first consider a simplified solution to the eigenvalue problem of Eq. (23) by neglecting the small terms $O(cq_x)$, $O(cq_y)$, and $O(q_x q_y)$. Afterwards, Eq. (23) is reduced to a minimally coupled (i.e., Peierls-substituted) Dirac Hamiltonian

$$H_{\boldsymbol{q}}^\xi = t\{\sigma_x[-\xi p q_x + (1+r)4cy] + \sigma_y(1-r)q_y\}, \tag{24}$$

where a strain-induced vector potential can be read off as $\boldsymbol{\mathcal{A}}^\xi = \xi\frac{4c}{p}(1+r)y\hat{x}$, giving rise to a uniform strain-induced pseudomagnetic field $\boldsymbol{\mathcal{B}}^\xi = \xi\frac{4c}{p}(1+r)\hat{z}$. The resulting strain-induced pseudo-Landau-levels read

$$E_n = \pm t\sqrt{n|c|8(1-r^2)}, \quad n = 0, 1, 2, \ldots, \tag{25}$$

which are dispersionless because the contribution from the inhomogeneous Fermi velocity is neglected. We are also able to solve the full eigenvalue problem of Eq. (23) and obtain the dispersive pseudo-Landau-levels (see Appendix C for details)

$$E_n^\xi = \pm t\sqrt{n|c|8[1-r^2+\xi p q_x(1-r)]}, \tag{26}$$

whose validity is justified by its good match to the numerical bands obtained by diagonalizing the nearest-neighbor

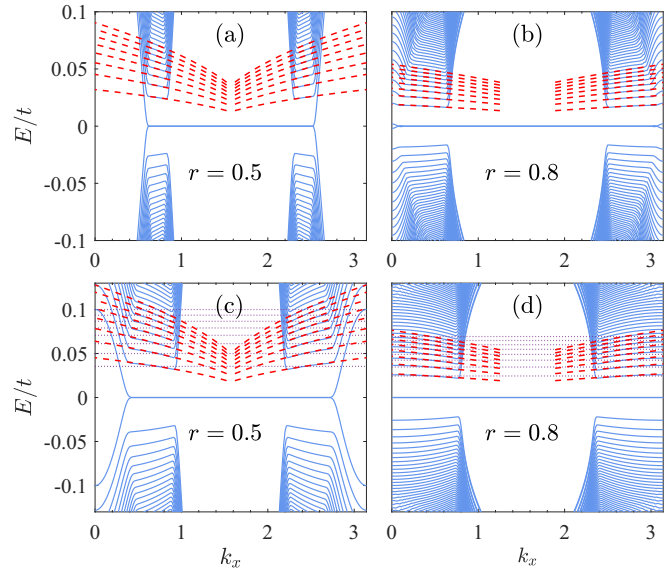

FIG. 7. The low-energy band structure of the nearest-neighbor tight-binding model on a staggered zero-flux square lattice under different strain patterns and r values. (a) Uniaxial strain, $r = 0.5$. (b) Uniaxial strain, $r = 0.8$. (c) Triaxial strain, $r = 0.5$. (d) Triaxial strain, $r = 0.8$. In all panels, the red dashed curves plot the analytical pseudo-Landau-levels [Eq. (21) for the uniaxial strain and Eq. (26) for the triaxial strain]. The width of the strip is $L_y = 600$, and the strain strength is $c = 0.5c_{\max}$.

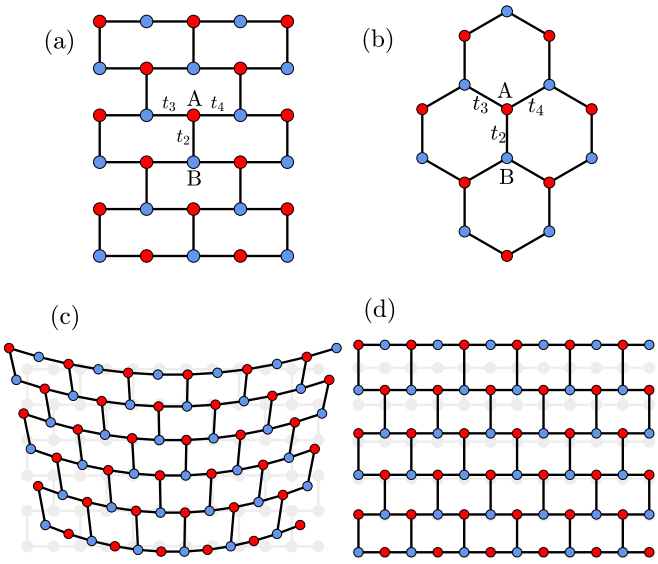

FIG. 8. Schematic plot of the staggered zero-flux square lattice with $t_1 = 0$ and the honeycomb lattice. The former is also known as the brick-wall lattice and is topologically equivalently to the latter. (a) Strain-free brick-wall lattice. (b) Strain-free honeycomb lattice. (c) Triaxially strained brick-wall lattice. (d) Uniaxially strained brick-wall lattice.

tight-binding model on the staggered zero-flux square lattice with triaxial strain [Figs. 7(c) and 7(d)].

VII. CONNECTION WITH THE HONEYCOMB LATTICE

In Sec. VI, we have shown that the staggered zero-flux square lattice hosts a pair of Dirac cones when $0 \leqslant t_1 < t$. In this section, we focus on the staggered zero-flux square with $t_1 = 0$ and study its connection with the honeycomb lattice. We first investigate the spectrum of a nearest-neighbor tight-binding model on the staggered zero-flux square lattice. Breaking the t_1 bond (i.e., the flux-carrying bond in the staggered π-flux square lattice), the staggered zero-flux square lattice is reduced to the so-called "brick-wall" lattice [Fig. 8(a)], which is topologically equivalent to a honeycomb lattice [Fig. 8(b)] because they can be transformed into one another through continuous lattice geometry variation. The band structure of the brick-wall lattice reads

$$E_{\boldsymbol{k}} = \pm t\sqrt{3 + 2\cos(2k_x) + 4\cos(k_x)\cos(k_y)}, \tag{27}$$

which is derived from the spectrum of Eq. (12) upon setting $t_1 = 0$. There are two Dirac points at $\boldsymbol{K}^{\xi} = (\xi\frac{2\pi}{3}, 0)$, around which the low-energy effective Hamiltonian is written as $H_{\boldsymbol{q}}^{\xi} = t(-\xi\sqrt{3}\sigma_x q_x + \sigma_y q_y)$, implying an anisotropic Dirac cone. In contrast, the band structure of the corresponding honeycomb lattice [1] is given by

$$E_{\boldsymbol{k}}^{\mathrm{h}} = \pm t\sqrt{3 + 2\cos(\sqrt{3}k_x) + 4\cos\left(\frac{\sqrt{3}}{2}k_x\right)\cos\left(\frac{3}{2}k_y\right)}. \tag{28}$$

Equation (28) also exhibits two Dirac points $\boldsymbol{K}^{\mathrm{h},\xi} = (\xi\frac{4\pi}{3\sqrt{3}}, 0)$, around which the low-energy effective Hamiltonian is written as $H_{\boldsymbol{q}}^{\mathrm{h},\xi} = \frac{3}{2}t(-\xi\sigma_x q_x + \sigma_y q_y)$, implying an isotropic Dirac cone. It is thus evident that the brick-wall lattice is linked to the honeycomb lattice under the following transformation:

$$k_x \to \frac{\sqrt{3}}{2}k_x,\ k_y \to \frac{3}{2}k_y, \tag{29}$$

which corresponds to the lattice geometry variation from the brick-wall lattice to the honeycomb lattice.

We next consider the strain effect. Here, our focus on the nonuniform triaxial strain, and the case of nonuniform uniaxial strain is similar. The low-energy effective Hamiltonian of the brick-wall lattice under the triaxial strain can be obtained directly by setting $r = 0$ in Eq. (24). It reads

$$H_{\boldsymbol{q}}^{\xi} = t\{\sigma_x[-\xi\sqrt{3}q_x + 4cy] + \sigma_y q_y\}. \tag{30}$$

For the honeycomb lattice, the effective Hamiltonian under the triaxial strain can be written as [41]

$$H_{\boldsymbol{q}}^{\xi} = \tfrac{3}{2}t\{\sigma_x[-\xi q_x + 2cy] + \sigma_y[q_y + \xi 2cx]\}. \tag{31}$$

Comparing Eq. (30) to Eq. (31), we find that the lattice geometry influences both the Fermi velocity and the strain-induced pseudovector potential. On the one hand, the Fermi velocities of the two lattices are connected by the transformation Eq. (29). On the other hand, the pseudovector potentials of the two lattices are different in gauge. While the pseudovector potential of the honeycomb lattice, $\boldsymbol{\mathcal{A}}^{\xi} = \xi(2cy, -2cx)$, is symmetric, the pseudovector potential of the brick-wall lattice only contains a nonzero x component $\mathcal{A}_x^{\xi} = 4\xi cy/\sqrt{3}$. The disappearance of $\mathcal{A}_y^{\xi}$ is attributed to the square geometry, where t_3 and t_4 are always equal under strain [Eq. (22)]. Although lattice geometry variation leads to discrepancy in the effective Hamiltonians, the resulting pseudo-Landau-levels can still be expressed using a general formula

$$E_n = \pm\hbar v_F\sqrt{8|c|n}, \quad n = 0, 1, 2, \ldots, \tag{32}$$

where $v_F = t/\hbar$ ($v_F = 3t/2\hbar$) for the brick-wall and honeycomb lattices, respectively.

Lastly, it is worth noting that the translational symmetry is completely broken by the triaxial strain in the honeycomb lattice. However, in the case of the brick-wall lattice, the translational symmetry along the x direction is preserved, because the strain-induced pseudovector potential adopts a Landau gauge [Eq. (30)]. This is evident from the fact that the hopping parameters, which are modulated by the triaxial strain, depend only on the y coordinate [Eq. (22)].

VIII. CONCLUSIONS

We have investigated the strain effects on columnar and staggered π-flux square lattices. Our analysis using low-energy effective theory reveals that strain applied to these π-flux square lattices does not induce pseudomagnetic fields, but rather leads to inhomogeneous Fermi velocities. We further explore alternative methods to generate pseudomagnetic fields in these systems. For columnar π-flux square lattices, pseudomagnetic fields can be created through nonuniform on-site potentials, while for staggered π-flux square lattices, pseudomagnetic fields require anisotropic hoppings. We have

validated the theoretical predictions of the pseudo-Landau-levels through numerical simulations using corresponding nearest-neighbor tight-binding models. The difference between pseudo-Landau-levels and ordinary Landau levels arising from magnetic fields is discussed.

Removing the flux from the staggered π-flux square lattice, we find that both uniaxial and triaxial strain can induce pseudomagnetic fields and dispersive pseudo-Landau-levels. Additionally, the strain-free and strained staggered zero-flux square lattices should in principle be more experimentally feasible than their π-flux counterparts. Further breaking the t_1 bond (i.e., the flux-carrying bond in the staggered π-flux square lattice) of the staggered zero-flux square lattice, we find that the resulting brick-wall lattice is topologically equivalent to the honeycomb lattice. While the strain-free band structures of these two lattices can be made equivalent by stretching and shrinking the Brillouin zone, the pseudomagnetic fields generated under the same triaxial strain are different in gauge. The triaxial-strain-deformed honeycomb lattice has a symmetric pseudovector potential, while the pseudovector potential in the triaxial-strain-deformed brick-wall lattice aligns along the x direction. These results expand the effect of strain to square geometries, further enhancing our comprehension of the strain-induced pseudomagnetic field. It is very possible that our strained lattices could be experimentally implemented in artificial platforms, such as optical lattices [51,52] or electrical circuits [53].

Recently, metamaterials have been instrumental in the study of pseudomagnetic fields and associated physical phenomena in honeycomb lattices. Experimental progress has been made in observing pseudo-Landau-levels on various artificial platforms [55–58], such as photonic [32,59,60], phononic [33,34,61], and topolectric [62,63] systems. Currently, there is no ideal two-dimensional quantum material with a square lattice structure similar to graphene that can perfectly replicate the honeycomb lattice. However, we anticipate that our theoretical findings can be validated through the utilization of artificially strained square lattices engineered using the aforementioned metamaterials. As an example, the two essential ingredients required to engineer the pseudomagnetic field, namely spatially nonuniform on-site potentials and anisotropic hoppings, can be effectively induced in topolectric circuits composed of simple elements such as capacitance and inductance [64,65]. The positive hoppings are achieved through the use of capacitors, while the negative hoppings are achieved by carefully selecting the appropriate inductors. The spatial variations in the hoppings required to generate the pseudomagnetic field can be created by connecting additional suitable inductors and capacitors. The on-site chemical potentials can be manipulated by applying distinct grounding elements to each site. Furthermore, a recent proposal suggests that a tight-binding model with arbitrary hopping amplitudes and phases can be constructed by extending a node in an LC circuit [65]. Given the rapid advancements in topolectric circuits, it is highly likely that our theoretical results pertaining to strained square lattices will be observed experimentally.

ACKNOWLEDGMENTS

The authors are indebted to E. Lantagne-Hurtubise, X.-X. Zhang, M. Franz, Z. Shi, and H.-Z. Lu for insightful discussions. J.S. and H.G. acknowledge support from the NSFC under Grants No. 11774019 and No. 12074022. T.L. acknowledges Guangdong Basic and Applied Basic Research Foundation under Grant No. 2022A1515111034. S.F. is supported by the National Key Research and Development Program of China under Grant No. 2021YFA1401803, and NSFC under Grants No. 11974051 and No. 12274036.

APPENDIX A: NONUNIFORM POTENTIAL INDUCED PSEUDO-LANDAU-LEVELS IN THE COLUMNAR π-FLUX SQUARE LATTICE

In Sec. IV of the main text, we have mentioned that a nonuniform potential produces pseudo-Landau-levels [Eq. (10)] in the columnar π-flux square lattice. We now explicitly derive Eq. (10) by solving the eigenvalue problem of Eq. (9).

Writing the wave function as $\Psi = e^{iq_y y}(\phi_A,\ \phi_B)^T$, the eigenvalue problem of Eq. (9) explicitly reads

$$\begin{aligned}(\xi q_y + U_0 x - \epsilon)\phi_A &= \frac{\partial}{\partial x}\phi_B,\\ (\xi q_y + U_0 x + \epsilon)\phi_B &= \frac{\partial}{\partial x}\phi_A,\end{aligned} \tag{A1}$$

where we define $\epsilon = \frac{E}{2t}$. Equation (A1) can be rewritten as

$$\begin{aligned}\left(\xi q_y + U_0 x - \frac{\partial}{\partial x}\right) f_1 &= \epsilon f_2,\\ \left(\xi q_y + U_0 x + \frac{\partial}{\partial x}\right) f_2 &= \epsilon f_1,\end{aligned} \tag{A2}$$

where we define new variables $f_1 = \phi_A + \phi_B$ and $f_2 = \phi_A - \phi_B$. Since $[\xi q_y + U_0 x + \frac{\partial}{\partial x}, \xi q_y + U_0 x - \frac{\partial}{\partial x}] = 2U_0$, we can define the following bosonic ladder operators:

$$\begin{aligned}\beta &= \frac{1}{\sqrt{2U_0}}\left(\xi q_y + U_0 x + \frac{\partial}{\partial x}\right),\\ \beta^\dagger &= \frac{1}{\sqrt{2U_0}}\left(\xi q_y + U_0 x - \frac{\partial}{\partial x}\right).\end{aligned} \tag{A3}$$

Making use of Eq. (A2), we obtain

$$2U_0 \beta^\dagger \beta f_2 = \epsilon^2 f_2. \tag{A4}$$

Note that $\beta^\dagger\beta$ is a bosonic number operator whose eigenvalues are $n = 0, 1, 2, \ldots$. We thus have $\epsilon = \pm\sqrt{2U_0 n}$, and the resulting pseudo-Landau-levels read

$$E_n = \pm 2t\sqrt{2U_0 n}, \quad n = 0, 1, 2, \ldots, \tag{A5}$$

which is labeled as Eq. (10) in the main text.

APPENDIX B: ANISOTROPIC HOPPINGS INDUCED PSEUDO-LANDAU-LEVELS IN THE STAGGERED π-FLUX SQUARE LATTICE

In Sec. V of the main text, we have mentioned that inhomogeneous anisotropic hoppings produce pseudo-Landau-levels [Eq. (17)] in the staggered π-flux square lattice. We now explicitly derive Eq. (17) by solving the eigenvalue problem of Eq. (16).

For simplicity, we perform a variable substitution $x \to x + \frac{2}{c}$ to Eq. (16). The resulting low-energy effective Hamiltonian becomes

$$\mathcal{H}_{\boldsymbol{q}}^{\xi} = 2t\left[-\frac{c}{2}\xi x \mathrm{i}\partial_x \sigma_x + \left(q_y - \xi - \xi\frac{c}{2}x\right)\sigma_y\right]. \tag{B1}$$

As $\mathrm{i}x\partial_x$ in Eq. (B1) is non-Hermitian, we need to replace it with a Hermitian operator, $\mathrm{i}x\partial_x \to \mathrm{i}(x\partial_x + \partial_x x)/2$. Writing the wave function as $\Psi = e^{iq_y y}(\phi_A, \phi_B)^T$, the eigenvalue problem of the Hermitianized effective Hamiltonian reads

$$\begin{aligned}\left[-i\frac{c}{2}\xi\left(x\partial_x + \frac{1}{2}\right) - i\left(q_y - \xi - \xi\frac{c}{2}x\right)\right]\phi_B = \epsilon\phi_A,\\ \left[-i\frac{c}{2}\xi\left(x\partial_x + \frac{1}{2}\right) + i\left(q_y - \xi - \xi\frac{c}{2}x\right)\right]\phi_A = \epsilon\phi_B,\end{aligned} \tag{B2}$$

where we have defined $\epsilon = \frac{E}{2t}$. The elimination of ϕ_A gives rise to a second-order ordinary differential equation with respect to ϕ_B as

$$\begin{aligned}&\left[x^2 - \frac{4(\xi q_y - 1) - c}{c}x + \frac{\Delta}{c^2} - \frac{1}{4}\right]\phi_B\\ &-(2x\phi_B' + x^2\phi_B'') = 0,\end{aligned} \tag{B3}$$

where we define $\Delta = 4[(\xi q_y - 1)^2 - \epsilon^2]$ for transparency.

We can then find the asymptotic solutions for $x \to 0$ and $x \to \pm\infty$, respectively. When approaching $x = 0$, we can neglect the $x^2\phi_B$ and $x\phi_B$ terms in Eq. (B3), leading to the following asymptotic ordinary differential equation:

$$\left(\frac{\Delta}{c^2} - \frac{1}{4}\right)\phi_B - (2x\phi_B' + x^2\phi_B'') = 0, \tag{B4}$$

which is a Cauchy-Euler equation with convergent solution $\phi_B \approx x^{-\frac{1}{2}+\frac{\sqrt{\Delta}}{|c|}}$. As $x \to \pm\infty$, only $x^2\phi_B$ and $x^2\phi_B''$ should be kept, leading to the following asymptotic ordinary differential equation:

$$\phi_B - \phi_B'' = 0. \tag{B5}$$

It is worth noting that the general solution to Eq. (B5), $\phi_B = Ae^x + Be^{-x}$, cannot converge simultaneously as $x \to -\infty$ and $x \to +\infty$. To guarantee the π flux, we require the engineered hopping t_3 to be positive. According to Eq. (15), this requirement mandates that the solution must converge as $x \to -\infty$ ($x \to +\infty$) if $c > 0$ ($c < 0$). Therefore, the convergent solution can be written as $\phi_B = e^{\mathrm{sgn}(c)x}$. With this *a posteriori* solution, we can express the full solution to Eq. (B3) as $\phi_B = e^{\mathrm{sgn}(c)x}x^{-\frac{1}{2}+\frac{\sqrt{\Delta}}{|c|}}u(x)$, which, upon substitution into Eq. (B3), yields

$$zu''(z) + (\gamma - z)u'(z) - \alpha u(z) = 0, \tag{B6}$$

where we define for transparency $\gamma = 1 + 2\sqrt{\Delta}/|c|$, $\alpha = \frac{1}{|c|}(\sqrt{\Delta} + 2\xi q_y + \frac{|c|-c}{2} - 2)$, and $z = -2\mathrm{sgn}(c)x$. Equation (B6) is a confluent hypergeometric equation with a regular singularity at $z = 0$, and it can be solved by the series expansion method. One solution reads

$$u(z) = 1 + \frac{\alpha}{\gamma}\frac{z}{1!} + \frac{\alpha(\alpha+1)}{\gamma(\gamma+1)}\frac{z^2}{2!} + \cdots, \tag{B7}$$

where $\gamma \neq 0, -1, -2, \ldots$. To make $u(z)$ a polynomial (and therefore finite) function, α should be zero or negative integers (i.e., $\alpha = -\nu$ with $\nu = 0, 1, 2, \ldots$). This constraint leads to the following expression for the eigenenergy:

$$E_n^{\xi} = \pm 2t\sqrt{n|c|(1 - \xi q_y)}, \tag{B8}$$

where $n = 0, 1, 2, \ldots$ ($n = 1, 2, \ldots$) for $c > 0$ ($c < 0$). This equation is labeled as Eq. (17) in the main text.

APPENDIX C: STRAIN-INDUCED PSEUDO-LANDAU-LEVELS IN THE STAGGERED ZERO-FLUX SQUARE LATTICE

In Sec. VI of the main text, we have mentioned that both uniaxial and triaxial strain produce pseudo-Landau-levels [Eqs. (21) and (26)] in the staggered zero-flux square lattice. We now explicitly derive Eqs. (21) and (26) by solving the eigenvalue problems of Eqs. (20) and (23), respectively.

We start from the eigenvalue problem of Eq. (20). For simplicity, we perform a variable substitution $y \to y + \frac{1-r-\xi pq_x}{2c}$, where $p = \sqrt{(3+r)(1-r)}$. The low-energy effective Hamiltonian [Eq. (20)] is changed to

$$H_{\boldsymbol{q}}^{\xi} = t\sigma_x\left[\frac{r-1}{2}\xi pq_x - (1+r)cy + \frac{r^2-1}{2}\right] + t\sigma_y \mathrm{i}2cy\partial_y. \tag{C1}$$

As the operator $\mathrm{i}y\partial_y$ in Eq. (C1) is non-Hermitian, we again apply the replacement $\mathrm{i}y\partial_y \to \mathrm{i}(y\partial_y + \partial_y y)/2$ to restore the Hermiticity. Writing the wave function as $\Psi = e^{iq_x x}(\phi_A,\ \phi_B)^T$, the eigenvalue problem of the Hermitianized effective Hamiltonian reads

$$\begin{aligned}\left[\frac{r-1}{2}\xi pq_x - (1+r)cy + \frac{r^2-1}{2} + 2cy\partial_y + c\right]\phi_B = \epsilon\phi_A,\\ \left[\frac{r-1}{2}\xi pq_x - (1+r)cy + \frac{r^2-1}{2} - 2cy\partial_y - c\right]\phi_A = \epsilon\phi_B,\end{aligned} \tag{C2}$$

where we have defined $\epsilon = E/t$. By eliminating ϕ_A, we obtain a second-order ordinary differential equation with respect to ϕ_B as

$$\begin{aligned}&\left\{\frac{(1+r)^2}{4}y^2 + \frac{(1+r)[2c - r^2 + 1 + (1-r)\xi pq_x]}{4c}y\right.\\ &\left.+\frac{\Delta}{4c^2} - \frac{1}{4}\right\}\phi_B - (2y\phi_B' + y^2\phi_B'') = 0,\end{aligned} \tag{C3}$$

where we define $\Delta = \frac{1}{4}[r^2 - 1 - (1-r)\xi pq_x]^2 - \epsilon^2$ for transparency.

Following the same strategy as in Appendix B, we first find the asymptotic solutions to Eq. (C3). For $y \to 0$, we neglect the $y^2\phi_B$ and $y\phi_B$ terms in Eq. (C3), resulting in the following asymptotic ordinary differential equation:

$$\left(\frac{\Delta}{4c^2} - \frac{1}{4}\right)\phi_B - (2y\phi_B' + y^2\phi_B'') = 0, \tag{C4}$$

whose convergent solution is $\phi_B \approx y^{-\frac{1}{2}+\frac{\sqrt{\Delta}}{2|c|}}$. As $y \to \pm\infty$, Eq. (C3) is simplified as

$$\frac{(1+r)^2}{4}\phi_B - \phi_B'' = 0, \tag{C5}$$

whose convergent solution is $\phi_B = e^{\mathrm{sgn}(c)\frac{(1+r)}{2}y}$. Consequently, the full solution to Eq. (C3) reads $\phi_B = y^{-\frac{1}{2}+\frac{\sqrt{\Delta}}{2|c|}} e^{\mathrm{sgn}(c)\frac{(1+r)}{2}y} u(y)$, which, upon plugging back into Eq. (C3), leads to the following confluent hypergeometric equation:

$$zu''(z) + (\gamma - z)u'(z) - \alpha u(z) = 0, \tag{C6}$$

where $\gamma = 1 - \frac{2\sqrt{\Delta}}{|c|}$, $\alpha = \frac{1}{|c|}(\sqrt{\Delta} - \xi pq_x + \frac{r^2-1}{2} + \frac{|c|-c}{2})$, and $z = -\mathrm{sgn}(c)(r+1)y$. As discussed in Appendix B, we require $\alpha = 0, -1, -2, \ldots$. This constraint requires the following eigenenergy:

$$E_n^\xi = \pm t\sqrt{2(1-r)}\sqrt{n|c|(\xi pq_x + 1 + r)}, \tag{C7}$$

which is labeled as Eq. (21) in the main text.

We now turn to study the eigenvalue problem of Eq. (23). For simplicity, we perform the variable substitution $y \to y - \frac{1-r-\xi pq_x}{2c(3+r)}$, where $p = \sqrt{(3+r)(1-r)}$. The low-energy effective Hamiltonian [Eq. (23)] is then mapped to

$$\begin{aligned} H_q^\xi =& t\sigma_x\left[\frac{(\xi pq_x + r - 1)^2 - p^2}{3+r} + 2c(2 + 2r + \xi pq_x)y\right] \\ &+ t\sigma_y 2c(3+r)(-\mathrm{i}y\partial_y). \end{aligned} \tag{C8}$$

To restore the Hermiticity of Eq. (C8), we again apply the replacement $\mathrm{i}y\partial_y \to \mathrm{i}(y\partial_y + \partial_y y)/2$. Writing the wave function as $\Psi = e^{iq_x x}(\phi_A,\ \phi_B)^T$, the eigenvalue problem of the Hermitianized effective Hamiltonian reads

$$\begin{aligned} &\left[\frac{(\xi pq_x + r - 1)^2 - p^2}{3+r} + 2c(2 + 2r + \xi pq_x)y \right. \\ &\quad \left. - 2c(3+r)y\partial_y - c(3+r)\right]\phi_B = \epsilon\phi_A, \\ &\left[\frac{(\xi pq_x + r - 1)^2 - p^2}{3+r} + 2c(2 + 2r + \xi pq_x)y \right. \\ &\quad \left. + 2c(3+r)y\partial_y + c(3+r)\right]\phi_A = \epsilon\phi_B, \end{aligned} \tag{C9}$$

where we have defined $\epsilon = E/t$. By eliminating ϕ_A, we arrive at a second-order ordinary differential equation with respect to ϕ_B as

$$\begin{aligned} &\left\{\frac{(2 + 2r + \xi pq_x)^2}{(3+r)^2}y^2 + \frac{(2 + 2r + \xi pq_x)}{(3+r)c} \right. \\ &\quad \times\left[\frac{(\xi pq_x + r)^2 + r^2}{(3+r)^2} + c - \frac{2(\xi pq_x + 1)}{(3+r)^2}\right]y \\ &\quad \left. + \frac{\Delta}{4c^2(3+r)^4} - \frac{1}{4}\right\}\phi_B - (y^2\phi_B'' + 2y\phi_B') = 0, \end{aligned} \tag{C10}$$

where $\Delta = [(\xi pq_x + r - 1)^2 - p^2]^2 - (3+r)^2\epsilon^2$ is defined for transparency.

Following the procedure solving Eqs. (B3) and (C3), we study the asymptotic solutions of Eq. (C10). For $y \to 0$, the terms associated with $y^2\phi_B$ and $y\phi_B$ in Eq. (C10) can be safely neglected, resulting in the following asymptotic ordinary differential equation:

$$\left[\frac{\Delta}{4c^2(3+r)^4} - \frac{1}{4}\right]\phi_B - (2y\phi_B' + y^2\phi_B'') = 0, \tag{C11}$$

whose convergent solution reads $\phi_B \approx y^{-\frac{1}{2}+\frac{\sqrt{\Delta}}{2|c|(3+r)^2}}$. As $y \to \pm\infty$, Eq. (C10) is reduced to

$$\frac{(2 + 2r + \xi pq_x)^2}{(3+r)^2}\phi_B - \phi_B'' = 0, \tag{C12}$$

whose convergent solution is $\phi_B = e^{\mathrm{sgn}(c)\frac{(2+2r+\xi pq_x)}{3+r}y}$. The full solution of Eq. (C10) can thus be written as $\phi_B = y^{-\frac{1}{2}+\frac{\sqrt{\Delta}}{2|c|(3+r)^2}} e^{\mathrm{sgn}(c)\frac{(2+2r+\xi pq_x)}{3+r}y} u(y)$, which, upon plugging back into Eq. (C10), leads to the following confluent hypergeometric equation:

$$zu''(z) + (\gamma - z)u'(z) - \alpha u(z) = 0, \tag{C13}$$

where $\gamma = [\sqrt{\Delta} + c^2(3+r)^2]/[2c(3+r)(2+2r+\xi pq_x)]$, $\alpha = [\sqrt{\Delta} - 2(\xi pq_x + 1) + 2c(3+r)^2 + (\xi pq_x + r)^2 + r^2]/[2c(3+r)^2]$, and $z = -\mathrm{sgn}(c)\frac{2(2+2r+\xi pq_x)}{3+r}y$. As discussed above, α should adopt zero or negative integers. This constraint requires the following eigenenergy:

$$E_n^\xi = \pm t\sqrt{n|c|8[1 - r^2 + \xi pq_x(1-r)]}, \tag{C14}$$

which is labeled as Eq. (26) in the main text.

[1] A. H. Castro Neto, F. Guinea, N. M. R. Peres, K. S. Novoselov, and A. K. Geim, The electronic properties of graphene, Rev. Mod. Phys. **81**, 109 (2009).

[2] F. de Juan, J. L. Mañes, and M. A. H. Vozmediano, Gauge fields from strain in graphene, Phys. Rev. B **87**, 165131 (2013).

[3] M. A. H. Vozmediano, M. I. Katsnelson, and F. Guinea, Gauge fields in graphene, Phys. Rep. **496**, 109 (2010).

[4] F. Guinea, M. I. Katsnelson, and A. K. Geim, Energy gaps and a zero-field quantum Hall effect in graphene by strain engineering, Nat. Phys. **6**, 30 (2010).

[5] F. Guinea, A. K. Geim, M. I. Katsnelson, and K. S. Novoselov, Generating quantizing pseudomagnetic fields by bending graphene ribbons, Phys. Rev. B **81**, 035408 (2010).

[6] M. Neek-Amal, L. Covaci, K. Shakouri, and F. M. Peeters, Electronic structure of a hexagonal graphene flake subjected to triaxial stress, Phys. Rev. B **88**, 115428 (2013).

[7] F. Guinea, B. Horovitz, and P. Le Doussal, Gauge field induced by ripples in graphene, Phys. Rev. B **77**, 205421 (2008).

[8] D.-B. Zhang, G. Seifert, and K. Chang, Strain-induced pseudomagnetic fields in twisted graphene nanoribbons, Phys. Rev. Lett. **112**, 096805 (2014).

[9] E. Lantagne-Hurtubise, X.-X. Zhang, and M. Franz, Dispersive Landau levels and valley currents in strained graphene nanoribbons, Phys. Rev. B **101**, 085423 (2020).

[10] N. Levy, S. A. Burke, K. L. Meaker, M. Panlasigui, A. Zettl, F. Guinea, A. H. C. Neto, and M. F. Crommie, Strain-induced

pseudo-magnetic fields greater than 300 Tesla in graphene nanobubbles, Science **329**, 544 (2010).

[11] C.-C. Hsu, M. L. Teague, J.-Q. Wang, and N.-C. Yeh, Nanoscale strain engineering of giant pseudo-magnetic fields, valley polarization, and topological channels in graphene, Sci. Adv. **6**, eaat9488 (2020).

[12] L. Meng, W.-Y. He, H. Zheng, M. Liu, H. Yan, W. Yan, Z.-D. Chu, K. Bai, R.-F. Dou, Y. Zhang *et al.*, Strain-induced one-dimensional Landau level quantization in corrugated graphene, Phys. Rev. B **87**, 205405 (2013).

[13] S.-Y. Li, K.-K. Bai, L.-J. Yin, J.-B. Qiao, W.-X. Wang, and L. He, Observation of unconventional splitting of Landau levels in strained graphene, Phys. Rev. B **92**, 245302 (2015).

[14] S.-Y. Li, Y. Su, Y.-N. Ren, and L. He, Valley polarization and inversion in strained graphene via pseudo-Landau levels, valley splitting of real Landau levels, and confined states, Phys. Rev. Lett. **124**, 106802 (2020).

[15] P. Nigge, A. C. Qu, E. Lantagne-Hurtubise, E. Mårsell, S. Link, G. Tom, M. Zonno, M. Michiardi, M. Schneider, S. Zhdanovich *et al.*, Room temperature strain-induced Landau levels in graphene on a wafer-scale platform, Sci. Adv. **5**, eaaw5593 (2019).

[16] P. Jia, W. Chen, J. Qiao, M. Zhang, X. Zheng, Z. Xue, R. Liang, C. Tian, L. He, Z. Di *et al.*, Programmable graphene nanobubbles with three-fold symmetric pseudo-magnetic fields, Nat. Commun. **10**, 3127 (2019).

[17] F. de Juan, M. Sturla, and M. A. H. Vozmediano, Space dependent Fermi velocity in strained graphene, Phys. Rev. Lett. **108**, 227205 (2012).

[18] Y. Chang, T. Albash, and S. Haas, Quantum Hall states in graphene from strain-induced nonuniform magnetic fields, Phys. Rev. B **86**, 125402 (2012).

[19] M. Settnes, S. R. Power, M. Brandbyge, and A.-P. Jauho, Graphene nanobubbles as valley filters and beam splitters, Phys. Rev. Lett. **117**, 276801 (2016).

[20] Z. Shi, H.-Z. Lu, and T. Liu, Pseudo Landau levels, negative strain resistivity, and enhanced thermopower in twisted graphene nanoribbons, Phys. Rev. Res. **3**, 033139 (2021).

[21] T. Liu and H.-Z. Lu, Analytic solution to pseudo-Landau levels in strongly bent graphene nanoribbons, Phys. Rev. Res. **4**, 023137 (2022).

[22] T. Liu, M. Franz, and S. Fujimoto, Quantum oscillations and Dirac-Landau levels in Weyl superconductors, Phys. Rev. B **96**, 224518 (2017).

[23] T. Matsushita, T. Liu, T. Mizushima, and S. Fujimoto, Charge/spin supercurrent and the Fulde-Ferrell state induced by crystal deformation in Weyl/Dirac superconductors, Phys. Rev. B **97**, 134519 (2018).

[24] G. Massarelli, G. Wachtel, J. Y. T. Wei, and A. Paramekanti, Pseudo-Landau levels of Bogoliubov quasiparticles in strained nodal superconductors, Phys. Rev. B **96**, 224516 (2017).

[25] E. M. Nica and M. Franz, Landau levels from neutral Bogoliubov particles in two-dimensional nodal superconductors under strain and doping gradients, Phys. Rev. B **97**, 024520 (2018).

[26] M. M. Nayga, S. Rachel, and M. Vojta, Magnon Landau levels and emergent supersymmetry in strained antiferromagnets, Phys. Rev. Lett. **123**, 207204 (2019).

[27] T. Liu and Z. Shi, Magnon quantum anomalies in Weyl ferromagnets, Phys. Rev. B **99**, 214413 (2019).

[28] T. Liu and Z. Shi, Strain-induced dispersive Landau levels: Application in twisted honeycomb magnets, Phys. Rev. B **103**, 144420 (2021).

[29] T. Liu, Z. Shi, H.-Z. Lu, and X. Xie, Chiral anomaly beyond fermionic paradigm, arXiv:2306.01446.

[30] J. Sun, N. Ma, T. Ying, H. Guo, and S. Feng, Quantum Monte Carlo study of honeycomb antiferromagnets under a triaxial strain, Phys. Rev. B **104**, 125117 (2021).

[31] J. Sun, H. Guo, and S. Feng, Magnon Landau levels in the strained antiferromagnetic honeycomb nanoribbons, Phys. Rev. Res. **3**, 043223 (2021).

[32] M. C. Rechtsman, J. M. Zeuner, A. Tünnermann, S. Nolte, M. Segev, and A. Szameit, Strain-induced pseudomagnetic field and photonic Landau levels in dielectric structures, Nat. Photon. **7**, 153 (2013).

[33] X. Wen, C. Qiu, Y. Qi, L. Ye, M. Ke, F. Zhang, and Z. Liu, Acoustic Landau quantization and quantum-Hall-like edge states, Nat. Phys. **15**, 352 (2019).

[34] C. Brendel, V. Peano, O. J. Painter, and F. Marquardt, Pseudomagnetic fields for sound at the nanoscale, Proc. Natl. Acad. Sci. (USA) **114**, E3390 (2017).

[35] V. Peri, M. Serra-Garcia, R. Ilan, and S. D. Huber, Axial-field-induced chiral channels in an acoustic Weyl system, Nat. Phys. **15**, 357 (2019).

[36] C. Poli, J. Arkinstall, and H. Schomerus, Degeneracy doubling and sublattice polarization in strain-induced pseudo-Landau levels, Phys. Rev. B **90**, 155418 (2014).

[37] Z.-q. Bao, J.-w. Ding, and J. Qi, Complex Landau levels and related transport properties in the strained zigzag graphene nanoribbons, Phys. Rev. B **107**, 125411 (2023).

[38] S. Rachel, I. Göthel, D. P. Arovas, and M. Vojta, Strain-induced Landau levels in arbitrary dimensions with an exact spectrum, Phys. Rev. Lett. **117**, 266801 (2016).

[39] F. Köhler and M. Vojta, Nodal semimetals in $d \geqslant 3$ to sharp pseudo-Landau levels by dimensional reduction, arXiv:2305.07051.

[40] T. Liu, Strain-induced pseudomagnetic field and quantum oscillations in kagome crystals, Phys. Rev. B **102**, 045151 (2020).

[41] J. Sun, T. Liu, Y. Du, and H. Guo, Strain-induced pseudo magnetic field in the $\alpha - T_3$ lattice, Phys. Rev. B **106**, 155417 (2022).

[42] A. Filusch and H. Fehske, Tunable valley filtering in dynamically strained $\alpha - T_3$ lattices, Phys. Rev. B **106**, 245106 (2022).

[43] A. B. Harris, T. C. Lubensky, and E. J. Mele, Flux phases in two-dimensional tight-binding models, Phys. Rev. B **40**, 2631(R) (1989).

[44] P. Delplace and G. Montambaux, Semi-Dirac point in the Hofstadter spectrum, Phys. Rev. B **82**, 035438 (2010).

[45] J.-M. Hou, W.-X. Yang, and X.-J. Liu, Massless Dirac fermions in a square optical lattice, Phys. Rev. A **79**, 043621 (2009).

[46] Y. Jia, H. Guo, Z. Chen, S.-Q. Shen, and S. Feng, Effect of interactions on two-dimensional Dirac fermions, Phys. Rev. B **88**, 075101 (2013).

[47] Z. Zhou, C. Wu, and Y. Wang, Mott transition in the π-flux $SU(4)$ Hubbard model on a square lattice, Phys. Rev. B **97**, 195122 (2018).

[48] S. M. Davis and M. S. Foster, Fractionalization waves in two-dimensional Dirac fermions: Quantum imprint from one dimension, Phys. Rev. Lett. **122**, 065302 (2019).

[49] Y.-X. Zhang, H.-M. Guo, and R. T. Scalettar, Charge density wave order on a π-flux square lattice, Phys. Rev. B **101**, 205139 (2020).

[50] D. Shaffer and L. H. Santos, Triplet pair density wave superconductivity on the π-flux square lattice, Phys. Rev. B **108**, 035135 (2023).

[51] M. Aidelsburger, M. Atala, M. Lohse, J. T. Barreiro, B. Paredes, and I. Bloch, Realization of the Hofstadter Hamiltonian with ultracold atoms in optical lattices, Phys. Rev. Lett. **111**, 185301 (2013).

[52] H. Miyake, G. A. Siviloglou, C. J. Kennedy, W. C. Burton, and W. Ketterle, Realizing the Harper Hamiltonian with laser-assisted tunneling in optical lattices, Phys. Rev. Lett. **111**, 185302 (2013).

[53] C. H. Lee, S. Imhof, C. Berger, F. Bayer, J. Brehm, L. W. Molenkamp, T. Kiessling, and R. Thomale, Topolectrical circuits, Commun. Phys. **1**, 39 (2018).

[54] M. Oliva-Leyva, J. E. Barrios-Vargas, and G. G. de la Cruz, Effective magnetic field induced by inhomogeneous Fermi velocity in strained honeycomb structures, Phys. Rev. B **102**, 035447 (2020).

[55] M. Yan, W. Deng, X. Huang, Y. Wu, Y. Yang, J. Lu, F. Li, and Z. Liu, Pseudomagnetic fields enabled manipulation of on-chip elastic waves, Phys. Rev. Lett. **127**, 136401 (2021).

[56] K. K. Gomes, W. Mar, W. Ko, F. Guinea, and H. C. Manoharan, Designer Dirac fermions and topological phases in molecular graphene, Nature (London) **483**, 306 (2012).

[57] M. Bellec, U. Kuhl, G. Montambaux, and F. Mortessagne, Tight-binding couplings in microwave artificial graphene, Phys. Rev. B **88**, 115437 (2013).

[58] M. Bellec, C. Poli, U. Kuhl, F. Mortessagne, and H. Schomerus, Observation of supersymmetric pseudo-Landau levels in strained microwave graphene, Light Sci. Appl. **9**, 146 (2020).

[59] M. Polini, F. Guinea, M. Lewenstein, H. C. Manoharan, and V. Pellegrini, Artificial honeycomb lattices for electrons, atoms and photons, Nat. Nanotechnol. **8**, 625 (2013).

[60] M. Jamotte, N. Goldman, and M. Di Liberto, Strain and pseudo-magnetic fields in optical lattices from density-assisted tunneling, Commun. Phys. **5**, 30 (2022).

[61] Z. Yang, F. Gao, Y. Yang, and B. Zhang, Strain-induced gauge field and Landau levels in acoustic structures, Phys. Rev. Lett. **118**, 194301 (2017).

[62] X.-X. Zhang and M. Franz, Non-Hermitian exceptional Landau quantization in electric circuits, Phys. Rev. Lett. **124**, 046401 (2020).

[63] H. T. Teo, S. Mandal, Y. Long, H. Xue, and B. Zhang, Pseudomagnetic suppression of non-Hermitian skin effect, arXiv:2307.05099.

[64] T. Hofmann, T. Helbig, C. H. Lee, M. Greiter, and R. Thomale, Chiral voltage propagation and calibration in a topolectrical Chern circuit, Phys. Rev. Lett. **122**, 247702 (2019).

[65] J. Dong, V. Juričić, and B. Roy, Topolectric circuits: Theory and construction, Phys. Rev. Res. **3**, 023056 (2021).